

Artículo aceptado en / *Paper accepted in*

REVISTA MEXICANA DE CIENCIAS GEOLÓGICAS



Versión preliminar / *Draft versión*

A novel methodology for geological modeling using a multilayer perceptron with supervised learning based on an implicit approach

por / *by*

**Heber Hernández, Martín Díaz-Viera, Sebastián Donaire,
Guillermo Sanchez-Vera, and Jorge Morales-Leal**

© 2026 The authors

<https://creativecommons.org/licenses/by/4.0/>



Manuscript received: May 21, 2025
Corrected manuscript received: April 15, 2026
Manuscript accepted: April 20, 2026
Draft version published: April 30, 2026

A novel methodology for geological modeling using a multilayer perceptron with supervised learning based on an implicit approach

Heber Hernández¹, Martín Díaz-Viera², Sebastián Donaire^{1,3},
Guillermo Sanchez-Vera^{1,3}, and Jorge Morales-Leal¹

¹ Facultad de Ingeniería y Negocios, Universidad Santo Tomás, Ejército Libertador 146, Santiago 8370003, Chile.

² Instituto Mexicano del Petróleo, Eje Central Lázaro Cárdenas No. 152, Ciudad de México 07730, México.

³ Departamento de Ingeniería Minera y Civil, Universidad Politécnica de Cartagena, Murcia, 30203, España.

* Corresponding author (H. Hernández): hhernandez9@santotomas.cl

ABSTRACT

This article presents a novel methodology for geological unit modeling, inspired by the theoretical conception of implicit geological modeling, but extending its capacity to incorporate covariates through a supervised learning method such as multi-layer perceptron. Based on a signed distance function applied to each drillhole sample, an auxiliary variable is generated which, together with spatial coordinates, is associated with the corresponding geological category. These data are used in a supervised training process, where the perceptron learns the spatial distribution of geological units. One of the main advantages of the model is its ease of incorporating covariates, allowing those with higher quality or sampling density to contribute to a more robust subsurface representation. Subsequently, both the auxiliary variable and the covariates are interpolated at the target coordinates. The trained perceptron assigns a geological class to each grid cell, and a post-processing step adjusts the contacts between units, enhancing geological continuity. The proposed methodology is validated using a synthetic dataset representing four stratified lithological units in a 2D grid. Each unit is associated with spatial coordinates and a secondary variable corresponding to rock density. From this grid, a 2.75% sample is extracted, equivalent to 11 irregularly spaced vertical drillholes, serving as the starting point for applying the method in a controlled environment. The results are compared with those from conventional implicit modeling using precision, recall, F1-score, and Kappa coefficient metrics, showing superior performance of the proposed method, honoring geological contacts, and improving the spatial distribution of lithological

units. The findings of this study provide a foundation for scaling the methodology, exploring new machine learning models, optimizing computational performance, and extending it to real 3D scenarios.

Keywords: geological modeling; geological implicit modelling; supervised learning; multi-layer perceptron.

RESUMEN

Este artículo presenta una novedosa metodología para modelamiento de unidades geológicas, inspirada en la concepción teórica del modelamiento geológico implícito, pero extendiendo su capacidad de incorporar covariables a través de un método de aprendizaje supervisado como el perceptrón multicapa. A partir de una función de distancia con signo aplicada a cada muestra de sondaje, se genera una variable auxiliar que, junto con las coordenadas espaciales, se asocia a la categoría geológica correspondiente. Estos datos se utilizan en un proceso de entrenamiento supervisado, en el que el perceptrón aprende la distribución espacial de las unidades geológicas. Una de las principales ventajas del modelo es la facilidad para incorporar covariables, permitiendo que aquellas de mayor calidad o densidad de muestreo contribuyan a una representación más robusta del subsuelo. Posteriormente, tanto la variable auxiliar como las covariables son interpoladas en las coordenadas objetivo. El perceptrón entrenado asigna una clase geológica a cada celda de la cuadrícula, y mediante un postproceso se ajustan los contactos entre unidades, mejorando la continuidad geológica. La validación de la propuesta metodológica se realiza utilizando una base de datos sintética que representa cuatro unidades litológicas estratificadas en una cuadrícula 2D. Cada unidad está asociada a coordenadas espaciales y a una variable secundaria correspondiente a la densidad de roca. A partir de esta cuadrícula, se extrae una muestra del 2,75%, equivalente a 11 sondajes verticales dispuestos de forma irregular, que constituyen el punto de partida para la aplicación del método en un entorno controlado. Los resultados se comparan con los del modelamiento implícito convencional mediante métricas de precisión, recall, F1-score y coeficiente Kappa, evidenciando un desempeño superior del método propuesto, respetando los contactos geológicos y mejorando la distribución espacial de las unidades litológicas. Los hallazgos de este estudio proporcionan una base para escalar la metodología, explorando nuevos modelos de aprendizaje automático, optimizando su desempeño computacional y extendiéndola a aplicaciones en escenarios reales 3D.

Palabras clave: *Modelamiento geológico, Modelamiento geológico implícito, Aprendizaje supervisado, Perceptrón multicapa.*

INTRODUCTION

Geological modeling is a computerized representation of various subsurface properties that aims to reliably portray an uncertain reality based on fragmentary information (Birch, 2014; Ma, 2019). These models are essential as a starting point for mineral resource estimation, as they allow the determination of rock distribution, alteration zones, and structural controls. This, in turn, facilitates the identification of elements or processes that contribute to the formation of mineralized systems (Wellmann & Caumon, 2018), providing a fundamental basis for conducting economic and technical evaluations of a deposit (Cavero *et al.*, 2016). The accuracy and level of detail of such models significantly affect mine planning and strategic decision-making throughout the project life cycle (Fookes, 1997). Uncertainty is a key focus and a critical condition for obtaining the best possible geological model estimations (Tacher *et al.*, 2006). Inadequate fitting of geological models, either in terms of tonnage or grade, can result in significant economic losses for a project. This, in turn, leads to overestimation of resources and underestimation of tonnage during mine reconciliation. The importance of these models extends beyond the mining sector into disciplines such as geophysics (Giraud *et al.*, 2024), geotechnics (de Rienzo *et al.*, 2008), hydrogeology (Bradbury *et al.*, 2007), and environmental management, making them a critical component in the efficient development of engineering projects and geological risk assessment.

Explicit modeling

Initially, geological modeling was developed almost exclusively using the explicit method. This involves the manual construction of three-dimensional models using computer-aided design tools, based on drillhole records, nodes, or surface study segments (J. Guo *et al.*, 2020). This methodology links digitized two-dimensional sections to later form a three-dimensional representation of geological phenomena (J. Guo *et al.*, 2018; Mallet, 1992; Ming *et al.*, 2010). However, despite its widespread use, this approach has significant limitations, including the introduction of biases due to subjective interpretation, challenges in representing complex geological features, high time costs, difficulty in auditing, and constraints in model updating (Cowan *et al.*, 2011; Martinelli & Tonetti, 2024a).

Implicit modeling

To overcome the limitations of explicit modeling, Cowan *et al.* (2002, 2003) proposed an approach that revolutionized geological model construction, known as implicit modeling. This method is based on the use of continuous mathematical functions to interpolate geological contacts from discrete drillhole data, allowing the generation of complex geological surfaces without intensive manual procedures. The distance function methodology (Osher & Fedkiw, 2003) is an implicit modeling technique that relies on interpolating signed distance functions within a geological domain (Deutsch & Wilde, 2013; McLennan & Deutsch, 2006). These functions quantify the separation between different geological units by considering their orientation, shape, and spatial extent. Positive values indicate that a point lies outside the unit, while negative values indicate it is inside. To estimate function values at unsampled locations, interpolation methods such as inverse distance weighting, radial basis function (RBF), Hermite radial basis function (HRBF), kriging, among others, can be used (J. Wang *et al.*, 2018). A threshold rule is then applied to define the boundaries between different geological units. This methodological evolution has significantly improved the accuracy of three-dimensional subsurface representation, reduced the subjectivity inherent in manual interpretation, and shortened the time required for geological data digitization and integration. Nevertheless, despite these advances, implicit modeling based on signed distance functions has notable limitations. One key issue is the inability to incorporate secondary information that complements the modeling of geological units, which is particularly problematic in contexts with sparse or irregularly distributed data, where the model tends to be unrepresentative and fragmented (Jessell *et al.*, 2010). A good geological model captures the formation history of a deposit. For instance, in the Flin Flon volcanogenic massive sulfide (VMS) deposit in Canada, the integration of lithogeochemical and geological data in a 3D model enabled the understanding of spatial relationships between mineralization, hydrothermal alteration, and fault planes, revealing how mineralization was redistributed during subsequent tectonic events (Schetselaar *et al.*, 2017). Other studies have implemented implicit modeling using radial basis functions to reconstruct mineralized bodies by integrating geological constraints that reflect structural trends, demonstrating advantages over explicit modeling (J. Guo *et al.*, 2022; Vollgger *et al.*, 2015; Zhong *et al.*, 2019). This technique has also been used for reconstructing structural systems, determining lithological contacts in space (Salvanus Yevalla *et al.*, 2024), and modeling aquifers and hydrogeological systems (D’Affonseca *et al.*, 2020). Some authors have compared implicit and explicit geological modeling (see Table 1), highlighting the strengths and limitations of each approach (Birch, 2014; Martinelli & Tonetti, 2024b). In this context, a combined strategy has been proposed to enhance

results, beginning with an initial implicit model that is then refined through manual review section by section along different axes (Collon & Caumon, 2017). However, this methodology has also been questioned, as it reintroduces the explicit model component, once again inheriting issues such as subjectivity and high dependence on the modeler's judgment.

Modeling Using Machine Learning

In recent years, the integration of Machine Learning (ML) techniques into geosciences has driven a transition from traditional physical and numerical approaches toward data-driven strategies (Brown *et al.*, 2000; J. T. Guo *et al.*, 2019; Rodriguez-Galiano *et al.*, 2015; Zhao *et al.*, 2024). ML has emerged as a promising alternative in this field due to its ability to identify complex patterns, efficiently integrate multiple sources of information, and improve the accuracy and robustness of generated models (Ashena & Thonhauser, 2015; Battalgazy *et al.*, 2023; Hillier *et al.*, 2021; Jia *et al.*, 2021; Kushwaha *et al.*, 2021; Yao *et al.*, 2020). The advancement of these techniques is reflected in the development of new modules within specialized geological modeling software (see Table 2), aimed at improving model accuracy while optimizing and accelerating the expert modeler's work.

Various studies have applied ML techniques to build geological models, selecting algorithms and input data based on the type of geological phenomenon being represented. For example, Smirnoff *et al.* (2008) and Wang *et al.* (2014) used support vector machines (SVM) to model sedimentary facies and shale lithofacies from well log and geological map data. Xiang *et al.* (2020) implemented random forests with geophysical and geological information to predict types of mineralization. Gonçalves *et al.* (2017, 2021) used maximum likelihood and Gaussian processes to model stratigraphic units and isovalues of potential fields. Jia *et al.* (2021) employed a stacking ensemble method to identify rock types using drilling and geophysical data. Bai & Tahmasebi (2020) trained a convolutional neural network to simulate lithofacies from flow images, while Hillier *et al.* (2021); Illarionov *et al.* (2022); Jiang *et al.*, (2021); Yao *et al.*, (2020); and Zhou *et al.*, (2019) applied various neural network architectures, including graph-based, generative, recurrent, and deep networks, to classify geological attributes and model subsurface structures in diverse contexts and applications. Unlike previous works, the present study introduces a novel contribution by incorporating an auxiliary variable into the model training process, grounded in the theoretical conception of implicit modeling through distance functions. The focus is not on comparing

models but on developing a generalizable methodology applicable to different geological problems and capable of integrating covariates into the modeling process.

This manuscript is organized as follows: Section 2 details the Implicit Multi-Layer Perceptron (IMLP) methodology; Section 3 presents an application case in a controlled synthetic scenario; Section 4 compares and discusses the results in relation to conventional implicit modeling. Finally, Section 5 presents the study's conclusions, along with potential pathways for scaling the proposed approach and opportunities for future improvement.

METHODOLOGY

The proposed methodology (see Figure 2) is sequentially divided into four stages, which together form a workflow hereafter referred to as IMLP.

Preprocessing, data preparation, and perceptron training:

The geological variable to be modeled is defined; it is categorical in nature and contains K categories, hereafter referred to as units. A secondary variable (covariate) spatially related to the units is established. If this covariate has a higher sampling frequency, its contribution becomes more significant. Spatial coordinates may represent a 2D or 3D space without altering the method's order or logic. The target grid is characterized by an origin coordinate, a number of cells, and a cell size for each axis. An auxiliary variable is constructed from the K units, where for all samples $\{z(u_i), i = 1, 2, 3, \dots, n\}$, an indicator vector of the K units is encoded in binary form:

$$I_k(u_i) = \begin{cases} 1, & \text{if } z(u_i)=k \\ 0, & \text{if } u_i \text{ otherwise} \end{cases} \text{ where } k = 1, 2, 3, \dots, K, \quad (1)$$

In this way, the elements of the vector take a value of one when they belong to the geological unit, while the remaining elements are encoded as zero. For each element, a signed distance function is applied, which yields a negative value if the samples are within the unit and a positive value otherwise:

$$d_k(u_i) = \begin{cases} -H(|u_i - u_j|), & \text{if } I_k(u_i)=1 \\ +H(|u_i - u_j|), & \text{if } I_k(u_i)=0 \end{cases}, \quad (2)$$

The function $H()$ is the square root of the squared differences between the locations $u_i - u_j$, which in 2D space is expressed as:

$$H(u_i - u_j) = \sqrt{(x_i - x_j)^2 + (y_i - y_j)^2}, \quad (3)$$

The prepared data corresponding to the geological units, spatial coordinates, auxiliary variable, and secondary variable are standardized (see Equation 4) and split into 80% for model training and 20% for testing.

$$z = \frac{x_i - \mu}{\sigma}, \quad (4)$$

Where x_i represents the original values of the variable, μ and σ represents the mean and standard deviation of the variable in the dataset, and z is the standardized value. The architecture of this model (see Figure 1) is composed of three types of layers. The input layer contains as many neurons as there are variables influencing the prediction of the geological units. The number of output neurons is equal to the number of units, K . The number of hidden layers and the number of neurons per layer depend on the specific characteristics of each problem. These hyperparameters, along with the activation function, learning rate, batch size, and optimizer, are determined using an iterative algorithm known as Grid Search (Belete & Huchaiah, 2022; Bischl *et al.*, 2023). This method systematically evaluates all possible combinations of hyperparameter values within a predefined grid and selects the one that optimizes a performance metric. Each neuron in the hidden layers is responsible for receiving information from the previous layer, processing it, and propagating it forward to reach the output layer. What happens in each neuron can be explained through the principle of the perceptron (Alberdi *et al.*, 2024; Rosenblatt, 1958).

$$\hat{y} = f(\sum_j x_j w_j + \theta), \quad (5)$$

where the x_j are the inputs to the unit, the w_j are the weights, θ is the bias term, f is the nonlinear activation function, and \hat{y} is the unit's activation. Extending this concept to multiple layers, the real outputs of the network are calculated:

$$\hat{y}_k(p) = f(\sum_{i=1}^m x_{jk}(p) \cdot w_{jk} + \theta_k), \quad (6)$$

Where m is the number of inputs for the neuron k from the output layer, and f is the activation function.

The objective is to minimize the error in estimation with respect to the known real value (label) by adjusting the weights.

$$E(w) = \min [f(\hat{y} - y)], \quad (7)$$

Where \hat{y} is the estimation value, y is the real value associated to input variables, and f is a cost function. The metrics used to validate the model are as follows: Precision, which measures the proportion of correct positive predictions out of all positive predictions; F1-Score is the harmonic mean of Precision and Recall; Recall measures the proportion of correctly identified positive samples among all actual positive samples, and F1-Score balances these two metrics; and finally, Cohen's Kappa, which measures the agreement between the predictions and the true labels, accounting for chance (See Appendix A).

Estimation of auxiliary and secondary variables

The auxiliary variable $d_k(u_i)$ with n observations is interpolated on the target grid using a RBF:

$$d * _k (u_i) = \sum_{i=1}^n \alpha_i \cdot \phi(\|\cdot\|), \quad (8)$$

Where $\|\cdot\|$ is the Euclidian norm in R^d , and d is the dimension of the space. The coefficients ($\alpha_1, \alpha_2, \dots, \alpha_n$) are determined by solving the linear system derived from:

$$d * (u_k) = \sum_{i=1}^n \alpha_i \cdot \phi(\|x_k - x_i\|), \quad 1 \leq k \leq n, \quad (9)$$

The choice of the function $\phi(r)$ can vary; linear function ($\phi(r) = r$), cubic function ($\phi(r) = r^3$), thin-plate splines ($\phi(r) = r^2 \log r$), among others, can be selected. In this work, our choice has been the linear-type RBF ($\phi(r) = r$). The secondary variable $Z(x_i)$ is estimated on the target grid using Ordinary Kriging (OK), assuming second-order stationarity, which allows the incorporation of a spatial variability model.

$$Z * (x_0) = \sum_{i=1}^n \lambda_i(x_0) \cdot Z(x_i), \quad (10)$$

Where $\lambda_i(x_0)$ are the weights of each value of $Z(x_i)$, which are optimal and minimize the estimation error variance, solved through a system of equations dependent on the covariances $C()$ ensuring linear unbiasedness with a term $\mu(x_0)$, which denotes a Lagrange multiplier:

$$\begin{cases} \sum_{i=1}^n \lambda_i(x_0) \cdot C(x_i - x_j) + \mu(x_0) = C(x_i - x_0), & i=1, \dots, n \\ \sum_{i=1}^n \lambda_i(x_0) = 1 \end{cases}, \quad (11)$$

Additionally, ordinary kriging provides the estimation error variance $\sigma_E^2(x_0)$, a useful aspect in the post-processing stage of this methodology, specifically for identifying areas where additional drilling is needed. The term σ^2 corresponds to the maximum variance of the spatial model.

$$\sigma_E^2(x_0) = \sigma^2 - \sum_{i=1}^n \lambda_i(x_0) \cdot C(x_i - x_0) - \mu(x_0), \quad (12)$$

Prediction of the geological unit

With the model trained and validated as described in Section 2.1, the prediction is performed on the target grid. This process requires knowledge of the predictor variables at the destination locations (see Section 2.2).

Post-processing:

The predicted geological units on the target grid serve as the basis for a sample extraction process, specifically in areas where the estimation variance of the secondary variable is highest. These extracted samples, in the form of drillholes, are added to the original database, forming a dense drilling mesh that is subsequently subjected to conventional implicit modeling.

APPLICATION

Construction of the synthetic database

A grid is defined covering an area of 1,000 meters along the X axis (Northing) and 300 meters along the Z axis (Elevation), with a cell size of 2.5 m x 2.5 m, resulting in a 400 x 120 matrix for a total of 48,000 cells. Each cell is assigned a rock type, numerically coded as 1, 2, 3, or 4, representing stratified layers understood as geological units. The shapes of these layers are generated using sine functions to create undulating boundaries, giving them a more natural and smooth contour.

$$R_i = C_i + A_i \cdot \sin\left(\frac{2\pi X}{\lambda_i} + \phi_i\right), \quad (13)$$

Where:

C_i is the mean elevation for R_i .

A_i is the undulation amplitude of R_i .

λ_i is the wavelength of R_i .

ϕ_i is the initial phase of R_i .

The stratified layers are superimposed and defined as:

$$R_i = \alpha_i \cdot R_{max} + A_i \cdot \sin\left(\frac{2\pi X}{\lambda_1} + \phi_1\right), \quad (14)$$

Where:

$$\alpha_i = \begin{cases} 1/4 & \text{for } i = \text{Layer 1, 3} \\ 1/2 & \text{for } i = \text{Layer 2} \\ 1/1 & \text{for } i = \text{Layer 4} \end{cases} \quad (15)$$

The transitions between layers are defined by conditions that determine the assigned rock type: [1 & {if} $R_i < R_1$; 2 & {if} $R_1 \leq R_i < R_2$; 3 & {if} $R_2 \leq R_i < R_3$; 4 & {if} $R_i \geq R_3$]. To create smooth transitions between layers, a transition width (w), is introduced, where cells in the transition zones are modified through additional conditions that adjust the rock type within the range ($[R_i - w, R_i + w]$) for each interface. A 2.75% sample is extracted from the grid in the form of 11 vertically oriented drillholes, spaced irregularly, with spatial coordinates (X, Z) and associated rock type (see Figure 3). Additionally, each rocktype is assigned a characteristic density sampled from a uniform distribution. This is done for practical purposes, to have a covariate that exhibits homogeneous behavior between geological units, but heterogeneous behavior within units. This partial information is used to carry out the implementation of the geological model.

Data preprocessing and preparation

The target variable, corresponding to rocktype, is divided into four units. Both the coordinates and rock density are variables directly obtained and measured from the mineral deposit. In this context, density serves as a secondary variable in the geological modeling process. As illustrated in Figure 4, the mean density exhibits distinctive characteristics, except in units 2 and 4, which notably do not have physical contact with each other (see Figure 3). Subsequently, the auxiliary variable defined as SDF_i is created at

the drillhole level. The SDF_i values for each rocktype in the target grid are obtained by interpolating using a radial basis function (see Figure 5). In parallel, the secondary variable must significantly contribute to the geological modeling process. Therefore, it is essential that it be related to the rocktype and that its modeling be carried out by an expert familiar with the area's geology and its interactions. If this variable is densely sampled, it becomes even more beneficial, as this reduces the uncertainty in its estimation. It is recommended to use geostatistical methods for its modeling, as these allow spatial continuity to be incorporated into the estimation, thereby improving accuracy. As shown in Figure 6, which depicts the experimental variograms alongside their respective theoretical fits for each direction, the modeling process begins by adjusting the theoretical curves based on the experimental data. This analysis demonstrates that density exhibits greater continuity in the horizontal direction than in the vertical one, which leads to the modeling of a geometric anisotropy: $\gamma(h) = 0.03\text{nugget} + 0.22\text{exponential}(450,70)$. Subsequently, OK is used as the estimator (see Figure 7), thereby completing the creation of the secondary variable. The sample dataset (see Table 3) is divided into 80% for training data and 20% for testing data, which corresponds to 1,056 and 264 data points, respectively. The target grid contains the spatial coordinates, the signed distance functions, and the secondary variable.

Model training and validation

The model achieves optimal results following a hyperparameter optimization using Grid Search across multiple combinations. The neural network architecture, both at the input and output layers, matches that shown in Figure 1, with two hidden layers of 128 neurons each, activated using a ReLU function. The output layer uses Softmax functions, and the Adaptive Moment Estimation (ADAM) optimizer is employed to adjust the network weights. When predicting domains on the training dataset, all performance metrics reach their maximum score, indicating that the model makes no errors in predicting the domains (see Figure 8).

Domain prediction on the target grid

With the validated MLP model, domain prediction is carried out on the target grid. These predictions serve as a basis for the extraction of new drillholes in under-sampled areas, specifically where the variance in the estimated rock density is high. It should be noted that this option can be approached with other

methods, such as those mentioned in (Wöhling *et al.*, 2016). The new synthetic drillholes, combined with the original ones, create a dense network of samples that are then used as input for an implicit geological modeling process. The visual result of the IMLP model (see Figure 9) preserves domain contacts at the drillhole level, which is achieved through the postprocessing step.

DISCUSSION

Conventional implicit modeling using the RBF interpolator presents a drawback: in areas with no data, some domains appear fragmented, creating satellite bodies that do not reflect the intrinsic continuity of the variable in nature (see Figure 10). This occurs because the method does not allow for the direct incorporation of additional information in the form of covariates. A common practice in the mining industry is to manually add control points for the domains at the modeler's discretion, effectively manipulating the modeling outcome. This results in a hybrid between implicit and explicit modeling, but it prevents automation, leading to longer processing times.

In the case of using another interpolator for the distance functions, such as OK, the outcome would be similar (see Table 4). Although OK allows for the incorporation of spatial variability, it cannot capture it effectively when only partial information is available. Consequently, the IMLP method, by enabling the integration of secondary information, whether more densely sampled or associated with lower uncertainty, yields a more realistic geological model.

Influence of drillhole layout on model quality

It is well known that sampling density and the spatial arrangement of samples, in this case, drillholes, directly affect modeling results (Hernandez *et al.*, 2020). The proper positioning of drillholes for subsurface sampling is closely related to the quality of the geological model. When drillholes are irregularly spaced or form clusters (see Figure 11, Scenario 7), evaluation metrics generally deteriorate (see Figure 12), reflecting a less accurate geological model. This issue, which affects any method relying solely on drillhole information, can be mitigated by the IMLP approach when supplemented with a more extensively sampled covariate. One example is the construction of lithological models using geophysical data as auxiliary information (Qi *et al.*, 2023).

Input Feature Selection for the IMLP Model

A questionable aspect of the proposed MLP architecture is the incorporation of absolute spatial coordinates. This arises because the IMLP employs a SDF for each geological unit, which inherently captures the spatial characteristics of the attribute being modeled. By computing the signed distance from each drilling sample to the contacts between geological units, these auxiliary variables encapsulate both the relative position of the samples with respect to boundaries and the underlying geometry of the units. Consequently, the MLP does not require absolute coordinates to learn spatial patterns, as the distance functions already encode these geometric relationships.

Key drawbacks of using coordinates in parallel with distance functions include:

- Informational redundancy, which disrupts weight optimization during ML model training.
- Increased computational complexity due to higher dimensionality.
- Artifact generation when extrapolating beyond the training domain, as models trained on drill-hole-specific coordinates may underperform outside their spatial range

In contrast, the interpolated nature of SDFs avoids this limitation. By eliminating the aforementioned redundancy, secondary variables interact directly with each SDF, enabling the perceptron to uncover more complex associations with reduced computational time and cost. This streamlined approach enhances both learning efficiency and model generalizability.

CONCLUSION

This article presents a novel geological modeling methodology that integrates the principles of implicit modeling through distance functions and enhances its performance using a MLP. This approach enables the incorporation of covariates, contributing to increased accuracy and representativeness of the resulting geological model. In the application case, rock density was used as a covariate, allowing the model to capture the complexity and continuity of geological units, mitigating limitations inherent to traditional interpolation methods that tend to fragment spatial representations. The performance analysis results, evaluated through various metrics such as precision, recall, F1-score, and Kappa, confirm that the IMLP method outperforms the IM-RBF model by an average of 93%. This suggests that the use of MLP architectures not only improves the prediction of geological units but also facilitates process automation,

reducing the time and effort required compared to hybrid methods. In summary, the proposed method represents a significant contribution to the field of geological modeling, offering a standardized, robust, and efficient approach that can be extended to real-world applications. Future work includes exploring variations in neural network types and other machine learning models, to be evaluated under the hypothesis that the IMLP model can be further improved. Additionally, future comparisons should be conducted in 3D cases using real geological unit data with more complex spatial distributions.

ABBREVIATIONS

- ADAM: Adaptive Moment Estimation
- IM: Implicit Modeling
- IMLP: Implicit Multi-Layer Perceptron
- m = Meters
- MLP: Multi-Layer Perceptron
- OK: Ordinary Kriging
- RBF: Radial Basis Function
- ReLU: Rectified Linear Unit
- SDF: Signed Distance Function

Funding. This article was not supported by any form of funding. No financial support, sponsorship, or external resources were received for its development.

APPENDIX A. EVALUATION METRICS

The mathematical foundations of the evaluation criteria are systematized below, distinguishing between class-prediction metrics (Precision, Recall, F1-Socre) and population-level reliability analysis (Kappa coefficient).

$$\text{Precision} = \frac{(TP)}{(TP)+(FP)}, \tag{A1}$$

$$\text{Recall} = \frac{(TP)}{(TP)+(FN)}, \tag{A2}$$

$$\text{F1-Score} = 2 \times \frac{\text{Precision} \times \text{Recall}}{\text{Precision} + \text{Recall}}, \tag{A3}$$

Where:

- TP: True Positives – correct positive predictions.
- FP: False Positives – incorrect positive predictions.
- TN: True Negatives – correct negative predictions.
- FN: False Negatives – incorrect negative predictions.

$$\kappa = \frac{p_o - p_e}{1 - p_e}, \tag{A4}$$

Where:

- (p_o): Observed agreement proportion (equivalent to Accuracy).
- (p_e): Expected agreement proportion by chance, calculated as:

$$p_e = \frac{(TP + FP) \times (TP + FN) + (TN + FP) \times (TN + FN)}{(TP + FP + TN + FN)^2}, \tag{A5}$$

REFERENCES

- Alberdi, E., Hernández, H., & Goti, A. (2024). Development of methods based on neural networks in the estimation of mineral resources. *Dyna (Spain)*, 99(3). <https://doi.org/10.6036/11077>
- Ashena, R., & Thonhauser, G. (2015). Application of Artificial Neural Networks in Geoscience and Petroleum Industry. In *Artificial Intelligent Approaches in Petroleum Geosciences* (pp. 127–166). Springer International Publishing. https://doi.org/10.1007/978-3-319-16531-8_4
- Bai, T., & Tahmasebi, P. (2020). Hybrid geological modeling: Combining machine learning and multiple-point statistics. *Computers and Geosciences*, 142. <https://doi.org/10.1016/j.cageo.2020.104519>
- Battalgazy, N., Valenta, R., Gow, P., Spier, C., & Forbes, G. (2023). Addressing Geological Challenges in Mineral Resource Estimation: A Comparative Study of Deep Learning and Traditional Techniques. *Minerals*, 13(7), 982. <https://doi.org/10.3390/min13070982>
- Belete, D. M., & Huchaiiah, M. D. (2022). Grid search in hyperparameter optimization of machine learning models for prediction of HIV/AIDS test results. *International Journal of Computers and Applications*, 44(9). <https://doi.org/10.1080/1206212X.2021.1974663>
- Birch, C. (2014). New systems for geological modelling - black box or best practice? *The Journal of The Southern African Institute of Mining and Metallurgy*, 144(12).
- Bischi, B., Binder, M., Lang, M., Pielok, T., Richter, J., Coors, S., Thomas, J., Ullmann, T., Becker, M., Boulesteix, A. L., Deng, D., & Lindauer, M. (2023). Hyperparameter optimization: Foundations, algorithms, best practices, and open challenges. In *Wiley Interdisciplinary Reviews: Data Mining and Knowledge Discovery* (Vol. 13, Issue 2). <https://doi.org/10.1002/widm.1484>
- Bradbury, K. R., Gotkowitz, M. B., & Hart, D. J. (2007, October). Evaluation of a bedrock aquitard for regional and local scale groundwater flow, threedimensional geologic mapping for groundwater applications. *Annual Meeting Geological Society of America*.
- Brown, W. M., Gedeon, T. D., Groves, D. I., & Barnes, R. G. (2000). Artificial neural networks: A new method for mineral prospectivity mapping. *Australian Journal of Earth Sciences*, 47(4). <https://doi.org/10.1046/j.1440-0952.2000.00807.x>
- Cavero, J., Orellana, N. H., Yemez, I., Singh, V., & Izaguirre, E. (2016). Importance of conceptual geological models in 3D reservoir modelling. *First Break*, 34(7). <https://doi.org/10.3997/1365-2397.2016010>
- Collon, P., & Caumon, G. (2017). 3D geomodelling in structurally complex areas - Implicit vs. explicit representations. *79th EAGE Conference and Exhibition 2017*. <https://doi.org/10.3997/2214-4609.201701144>
- Cowan, E., Beatson, R., Fright, W., McLennan, T., & Mitchell, T. (2002). Rapid geological modelling. *Applied Structural Geology for Mineral Exploration and Mining, International Symposium*, 39–44.
- Cowan, E., Beatson, R., Ross, H., Fright, W., McLennan, T., Evans, T., Carr, J., Lane, R., Bright, D., Gillman, A., Oshurst, P., & Titley, M. (2003). Practical Implicit Geological Modelling. *AusIMM 5th International Mining Geology Conference*, 88–89.

- D’Affonseca, F. M., Finkel, M., & Cirpka, O. A. (2020). Combining implicit geological modeling, field surveys, and hydrogeological modeling to describe groundwater flow in a karst aquifer. *Hydrogeology Journal*, 28(8), 2779–2802. <https://doi.org/10.1007/s10040-020-02220-z>
- de Rienzo, F., Oreste, P., & Pelizza, S. (2008). Subsurface geological-geotechnical modelling to sustain underground civil planning. *Engineering Geology*, 96(3–4), 187–204. <https://doi.org/10.1016/j.enggeo.2007.11.002>
- Deutsch, C. V., & Wilde, B. J. (2013). Modeling multiple coal seams using signed distance functions and global kriging. *International Journal of Coal Geology*, 112, 87–93. <https://doi.org/10.1016/j.coal.2012.11.013>
- Fookes, P. G. (1997). Geology for Engineers: the Geological Model, Prediction and Performance. *Quarterly Journal of Engineering Geology*, 30(4), 293–424. <https://doi.org/10.1144/GSL.QJEG.1997.030.P4.02>
- Giraud, J., Caumon, G., Grose, L., Ogarko, V., & Cupillard, P. (2024). Integration of automatic implicit geological modelling in deterministic geophysical inversion. *Solid Earth*, 15(1), 63–89. <https://doi.org/10.5194/se-15-63-2024>
- Gonçalves, Í. G., Guadagnin, F., Kumaira, S., & Da Silva, S. L. (2021). A machine learning model for structural trend fields. *Computers and Geosciences*, 149. <https://doi.org/10.1016/j.cageo.2021.104715>
- Gonçalves, Í. G., Kumaira, S., & Guadagnin, F. (2017). A machine learning approach to the potential-field method for implicit modeling of geological structures. *Computers and Geosciences*, 103. <https://doi.org/10.1016/j.cageo.2017.03.015>
- Guerra, H. H., Alberdi, E., & Goti, A. (2020). Influence of the sampling density in the coestimation error of a regionalized locally stationary variable. *Minerals*, 10(2). <https://doi.org/10.3390/min10020090>
- Guo, J. T., Liu, Y. H., Han, Y. F., & Wang, X. L. (2019). Implicit 3D Geological Modeling Method for Borehole Data Based on Machine Learning. *Dongbei Daxue Xuebao/Journal of Northeastern University*, 40(9). <https://doi.org/10.12068/j.issn.1005-3026.2019.09.021>
- Guo, J., Wang, J., Wu, L., Liu, C., Li, C., Li, F., Lin, M., Jessell, M. W., Li, P., Dai, X., & Tang, J. (2020). Explicit-implicit-integrated 3-D geological modelling approach: A case study of the Xianyan Demolition Volcano (Fujian, China). *Tectonophysics*, 795, 228648. <https://doi.org/10.1016/j.tecto.2020.228648>
- Guo, J., Wang, J., Wu, L., Zhu, W., Jessell, M., Li, C., Li, F., & Hu, H. (2022). Automatic and dynamic updating of three-dimensional ore body models from borehole and excavation data using the implicit function HRBF. *Ore Geology Reviews*, 148, 105018. <https://doi.org/10.1016/j.oregeorev.2022.105018>
- Guo, J., Wu, L., Zhou, W., Li, C., & Li, F. (2018). Section-constrained local geological interface dynamic updating method based on the HRBF surface. *Journal of Structural Geology*, 107, 64–72. <https://doi.org/10.1016/j.jsg.2017.11.017>
- Hillier, M., Wellmann, F., Brodaric, B., de Kemp, E., & Schetselaar, E. (2021). Three-Dimensional Structural Geological Modeling Using Graph Neural Networks. *Mathematical Geosciences*, 53(8), 1725–1749. <https://doi.org/10.1007/s11004-021-09945-x>

- Illarionov, E., Temirchev, P., Voloskov, D., Kostoev, R., Simonov, M., Pissarenko, D., Orlov, D., & Koroteev, D. (2022). End-to-end neural network approach to 3D reservoir simulation and adaptation. *Journal of Petroleum Science and Engineering*, 208. <https://doi.org/10.1016/j.petrol.2021.109332>
- Jessell, M. W., Ailleres, L., & de Kemp, E. A. (2010). Towards an integrated inversion of geoscientific data: What price of geology? *Tectonophysics*, 490(3–4), 294–306. <https://doi.org/10.1016/j.tecto.2010.05.020>
- Jia, R., Lv, Y., Wang, G., Carranza, E. J. M., Chen, Y., Wei, C., & Zhang, Z. (2021). A stacking methodology of machine learning for 3D geological modeling with geological-geophysical datasets, Laochang Sn camp, Gejiu (China). *Computers and Geosciences*, 151. <https://doi.org/10.1016/j.cageo.2021.104754>
- Jiang, Z., Mallants, D., Gao, L., Munday, T., Mariethoz, G., & Peeters, L. (2021). Sub3DNet1.0: A deep-learning model for regional-scale 3D subsurface structure mapping. *Geoscientific Model Development*, 14(6). <https://doi.org/10.5194/gmd-14-3421-2021>
- Kushwaha, P. K., Maurya, S. P., Rai, P., & Singh, N. P. (2021). Estimation of subsurface rock properties from seismic inversion and geo-statistical methods over F3-block, Netherland. *Exploration Geophysics*, 52(3), 258–272. <https://doi.org/10.1080/08123985.2020.1815528>
- Ma, Y. Z. (2019). Introduction to Geological and Reservoir Modeling. In *Quantitative Geosciences: Data Analytics, Geostatistics, Reservoir Characterization and Modeling* (pp. 333–349). Springer International Publishing. https://doi.org/10.1007/978-3-030-17860-4_14
- Mallet, J.-L. (1992). Discrete smooth interpolation in geometric modelling. *Computer-Aided Design*, 24(4), 178–191. [https://doi.org/10.1016/0010-4485\(92\)90054-E](https://doi.org/10.1016/0010-4485(92)90054-E)
- Martinelli, M., & Tonetti, M. (2024a). Combination of Explicit and Implicit Approaches for 3D Geomodelling of Tailings Deposits Using Sparse Data. *85th EAGE Annual Conference & Exhibition*, 1–5. <https://doi.org/10.3997/2214-4609.202410078>
- Martinelli, M., & Tonetti, M. (2024b). Combination of Explicit and Implicit Approaches for 3D Geomodelling of Tailings Deposits Using Sparse Data. *85th EAGE Annual Conference & Exhibition*, 1–5. <https://doi.org/10.3997/2214-4609.202410078>
- Mclennan, J. A., & Deutsch, C. V. (2006). Implicit Boundary Modeling (BOUNDSIM). *Proceedings of the 2007 APCOM Symposium*.
- Ming, J., Pan, M., Qu, H., & Ge, Z. (2010). GISIS: A 3D geological multi-body modeling system from netty cross-sections with topology. *Computers & Geosciences*, 36(6), 756–767. <https://doi.org/10.1016/j.cageo.2009.11.003>
- Osher, S., & Fedkiw, R. (2003). Signed Distance Functions. In *Level Set Methods and Dynamic Implicit Surfaces* (pp. 17–22). Springer New York. https://doi.org/10.1007/0-387-22746-6_2
- Qi, G., Meng, G., Yan, J., Tang, H., & Xue, R. (2023). Three-Dimensional Geological–Geophysical Modeling and Prospecting Indications of the Ashele Ore Concentration Area in Xinjiang Based on Irregular Sections. *Minerals*, 13(7). <https://doi.org/10.3390/min13070984>
- Rodriguez-Galiano, V., Sanchez-Castillo, M., Chica-Olmo, M., & Chica-Rivas, M. (2015). Machine learning predictive models for mineral prospectivity: An evaluation of neural networks, random

- forest, regression trees and support vector machines. *Ore Geology Reviews*, 71, 804–818. <https://doi.org/10.1016/j.oregeorev.2015.01.001>
- Rosenblatt, F. (1958). The perceptron: A probabilistic model for information storage and organization in the brain. *Psychological Review*, 65(6). <https://doi.org/10.1037/h0042519>
- Salvanus Yevalla, G.-M., Rodrigue, E. S., Ndoh, N. E., & Tabod, T. C. (2024). Characterization of subsurface geology and hydrogeology in Kribi -Cameroon using electrical resistivity soundings and 3D-Implicit modelling: Baseline for groundwater resource management. *Groundwater for Sustainable Development*, 25, 101163. <https://doi.org/10.1016/j.gsd.2024.101163>
- Schetselaar, E., Ames, D., & Grunsky, E. (2017). Integrated 3D Geological Modeling to Gain Insight in the Effects of Hydrothermal Alteration on Post-Ore Deformation Style and Strain Localization in the Flin Flon Volcanogenic Massive Sulfide Ore System. *Minerals*, 8(1), 3. <https://doi.org/10.3390/min8010003>
- Smirnoff, A., Boisvert, E., & Paradis, S. J. (2008). Support vector machine for 3D modelling from sparse geological information of various origins. *Computers and Geosciences*, 34(2). <https://doi.org/10.1016/j.cageo.2006.12.008>
- Tacher, L., Pomian-Szrednicki, I., & Parriaux, A. (2006). Geological uncertainties associated with 3-D subsurface models. *Computers & Geosciences*, 32(2), 212–221. <https://doi.org/10.1016/j.cageo.2005.06.010>
- Vollgger, S. A., Cruden, A. R., Ailleres, L., & Cowan, E. J. (2015). Regional dome evolution and its control on ore-grade distribution: Insights from 3D implicit modelling of the Navachab gold deposit, Namibia. *Ore Geology Reviews*, 69, 268–284. <https://doi.org/10.1016/j.oregeorev.2015.02.020>
- Wang, G., Carr, T. R., Ju, Y., & Li, C. (2014). Identifying organic-rich Marcellus Shale lithofacies by support vector machine classifier in the Appalachian basin. *Computers and Geosciences*, 64. <https://doi.org/10.1016/j.cageo.2013.12.002>
- Wang, J., Zhao, H., Bi, L., & Wang, L. (2018). Implicit 3D modeling of ore body from geological boreholes data using hermite radial basis functions. *Minerals*, 8(10). <https://doi.org/10.3390/min8100443>
- Wellmann, F., & Caumon, G. (2018). 3-D Structural geological models: Concepts, methods, and uncertainties. In *Advances in Geophysics* (Vol. 59). <https://doi.org/10.1016/bs.agph.2018.09.001>
- Wöhling, T., Geiges, A., & Nowak, W. (2016). Optimal Design of Multitype Groundwater Monitoring Networks Using Easily Accessible Tools. *Groundwater*, 54(6). <https://doi.org/10.1111/gwat.12430>
- Xiang, J., Xiao, K., Carranza, E. J. M., Chen, J., & Li, S. (2020). 3D Mineral Prospectivity Mapping with Random Forests: A Case Study of Tongling, Anhui, China. *Natural Resources Research*, 29(1). <https://doi.org/10.1007/s11053-019-09578-2>
- Yao, J., Liu, Q., Liu, W., Liu, Y., Chen, X., & Pan, M. (2020). 3D Reservoir Geological Modeling Algorithm Based on a Deep Feedforward Neural Network: A Case Study of the Delta Reservoir of Upper Urho Formation in the X Area of Karamay, Xinjiang, China. *Energies*, 13(24), 6699. <https://doi.org/10.3390/en13246699>
- Zhao, T., Wang, S., Ouyang, C., Chen, M., Liu, C., Zhang, J., Yu, L., Wang, F., Xie, Y., Li, J., Wang, F., Grunwald, S., Wong, B. M., Zhang, F., Qian, Z., Xu, Y., Yu, C., Han, W., Sun, T., ... Wang, L.

(2024). Artificial intelligence for geoscience: Progress, challenges, and perspectives. *The Innovation*, 5(5), 100691. <https://doi.org/10.1016/J.XINN.2024.100691>

Zhong, D., Wang, L., BI, L., & JIA, M. (2019). Implicit modeling of complex orebody with constraints of geological rules. *Transactions of Nonferrous Metals Society of China*, 29(11), 2392–2399. [https://doi.org/10.1016/S1003-6326\(19\)65145-9](https://doi.org/10.1016/S1003-6326(19)65145-9)

Zhou, C., Ouyang, J., Ming, W., Zhang, G., Du, Z., & Liu, Z. (2019). A stratigraphic prediction method based on machine learning. *Applied Sciences (Switzerland)*, 9(17). <https://doi.org/10.3390/app9173553>

FIGURES

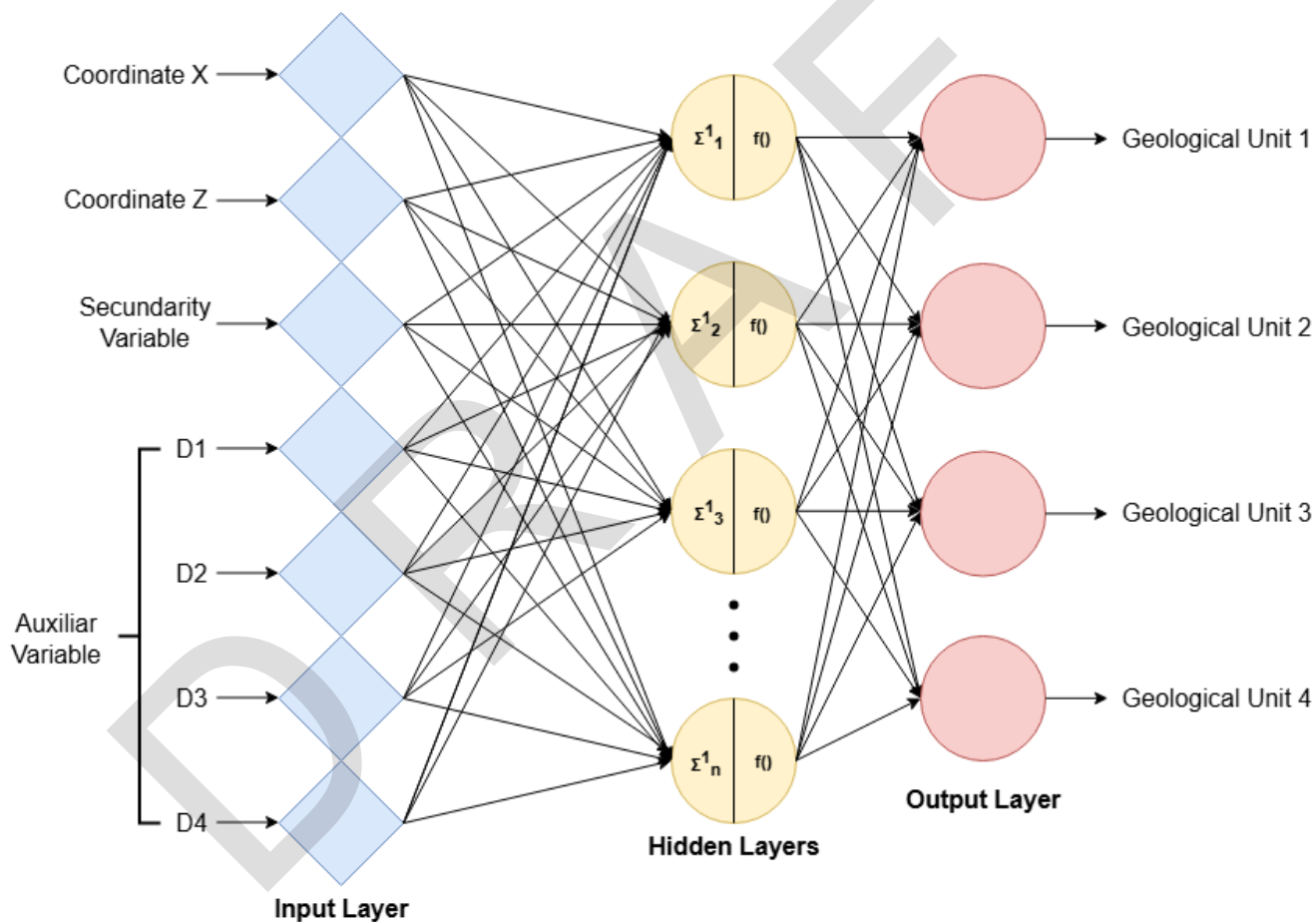


Figure 1. MLP architecture per four geological units.

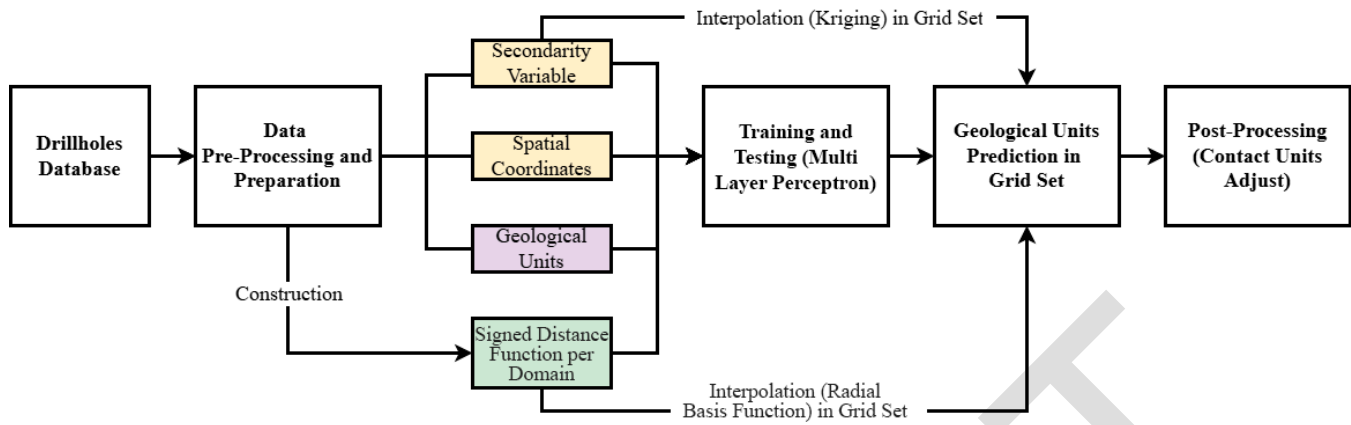


Figure 2. Methodology flowchart proposed (IMLP).

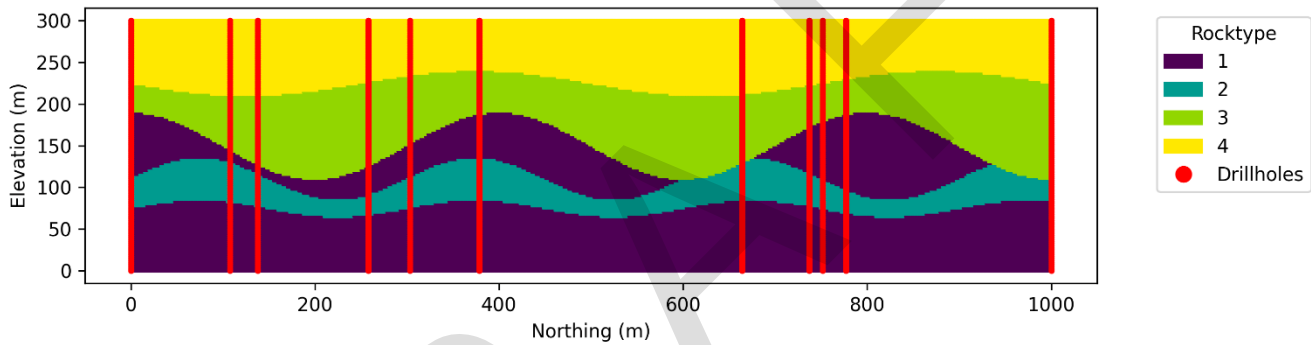


Figure 3. Rocktype (synthetic background) and drillholes sample position.

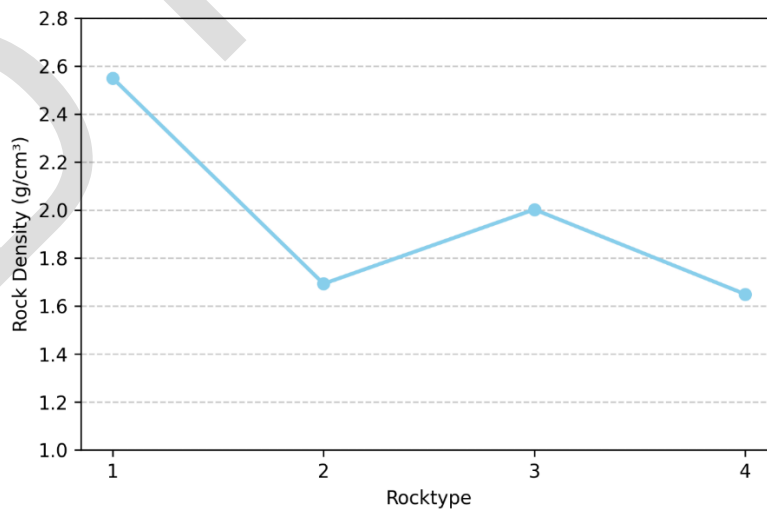


Figure 4. Rock density mean per domain (rocktype).

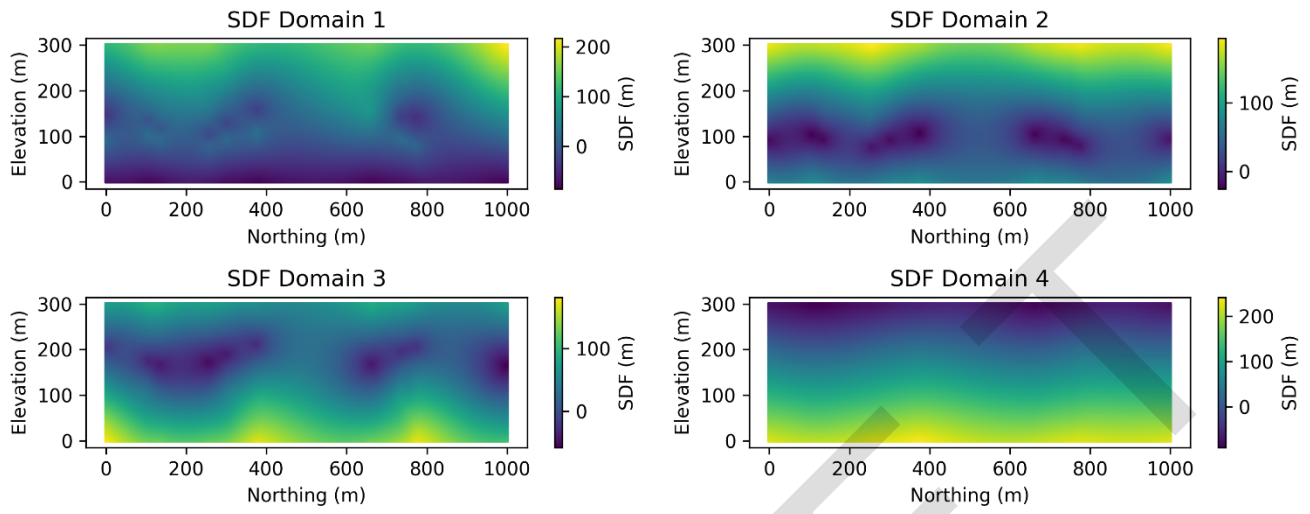


Figure 5. SDF per domain in target grid set.

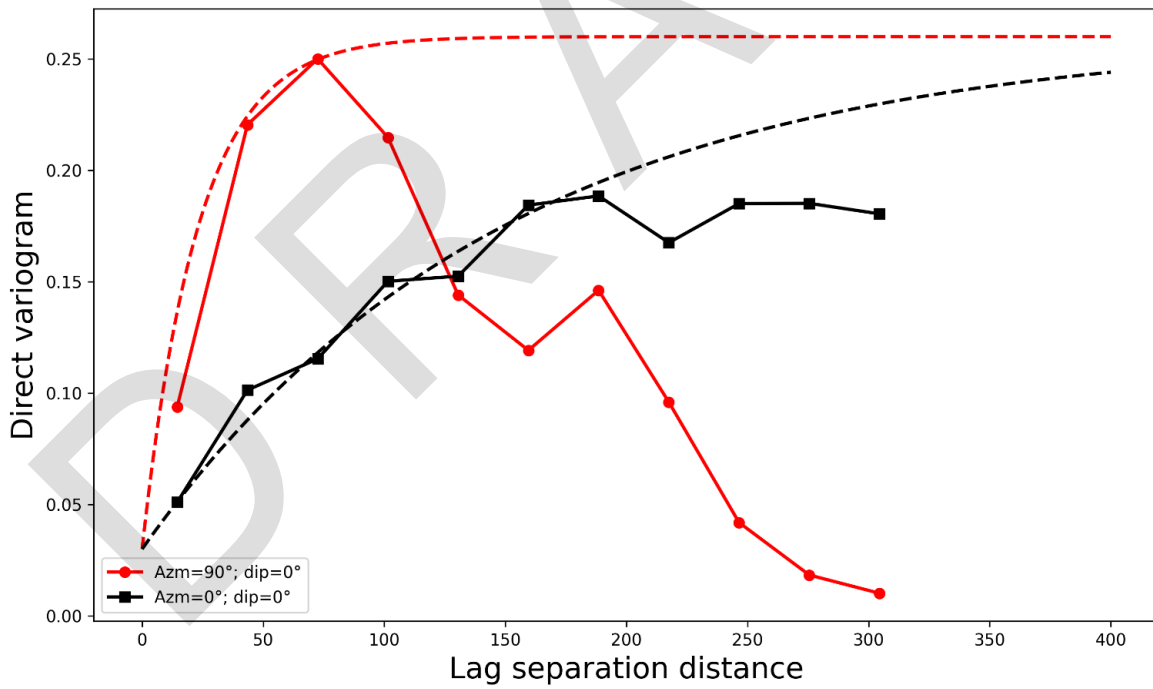


Figure 6. Rock density variogram.

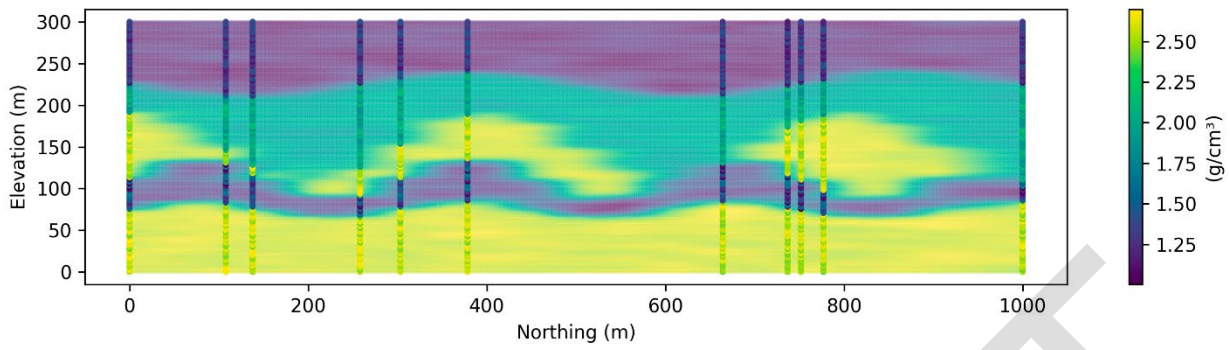


Figure 7. Rock density drillholes and OK estimated.

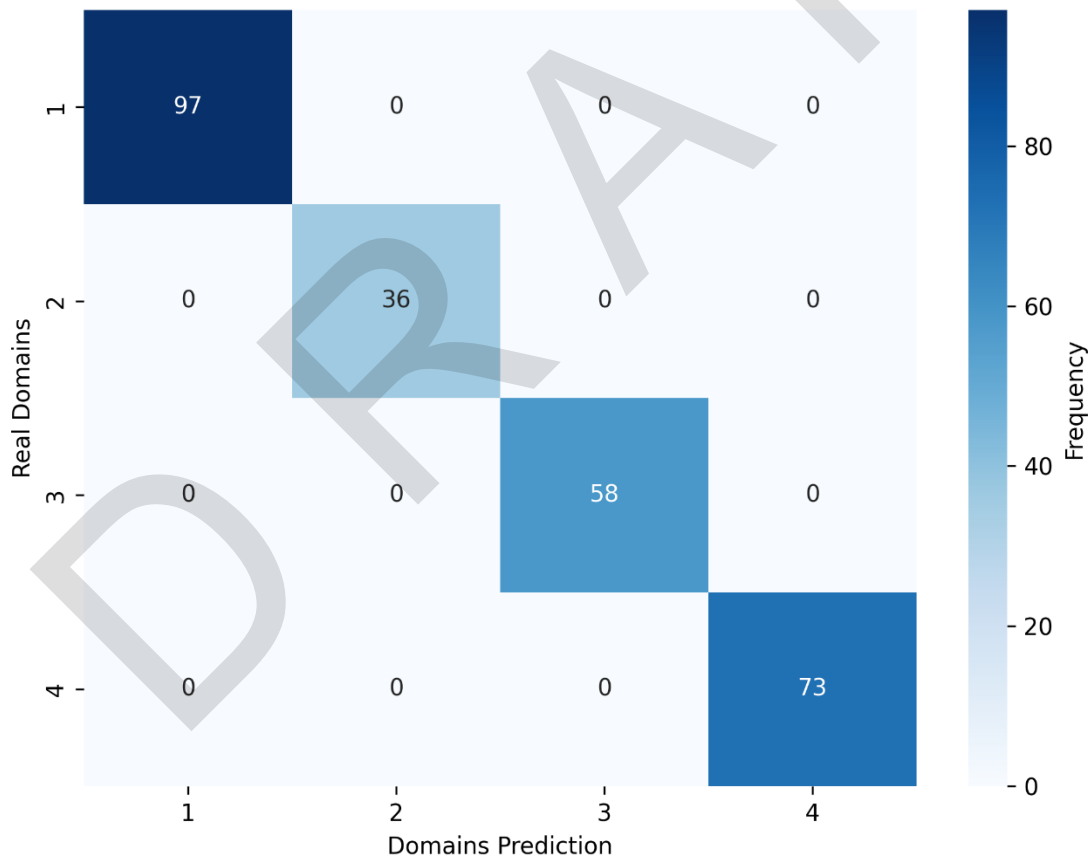


Figure 8. Confusion matrix of the MLP on the training dataset.

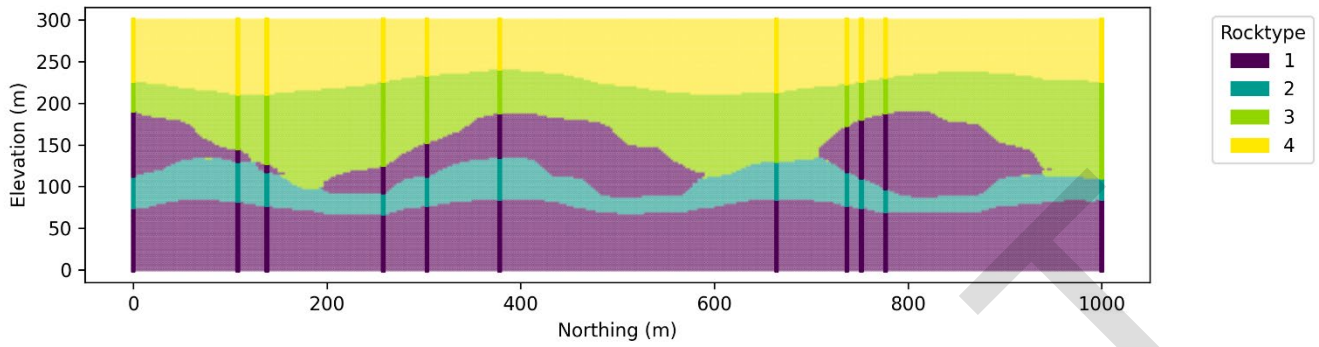


Figure 9. IMLP applied in rocktype.

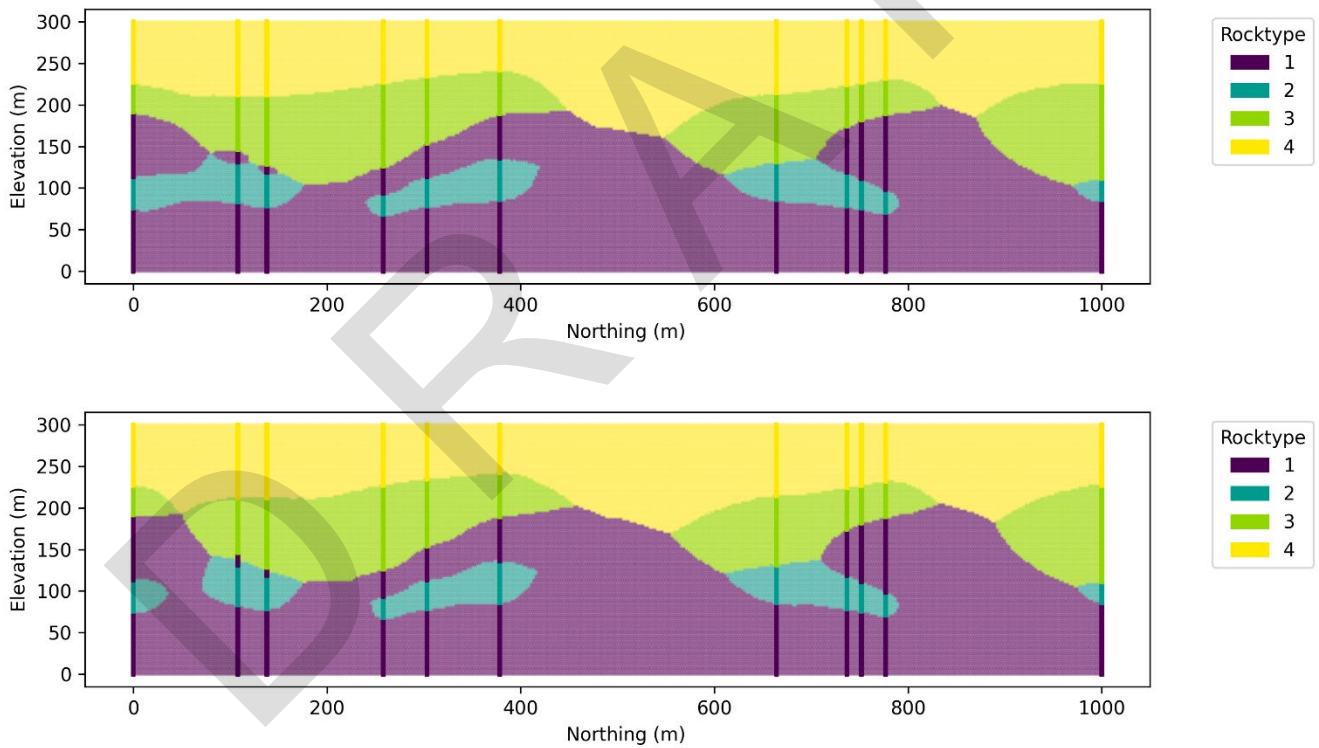


Figure 10. Implicit modeling applied in Rocktype (RBF upper and OK lower).

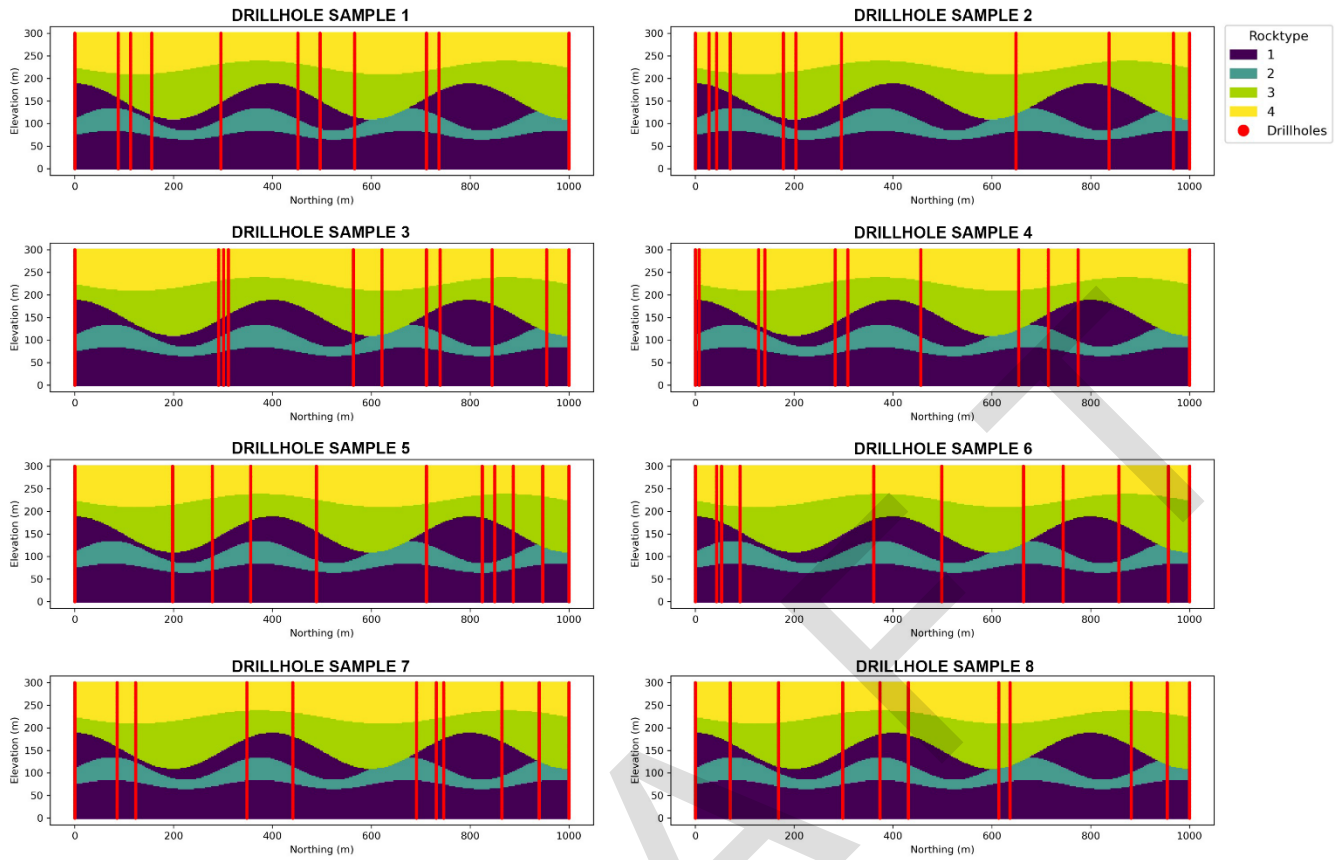


Figure 11. Random sampling scenarios.

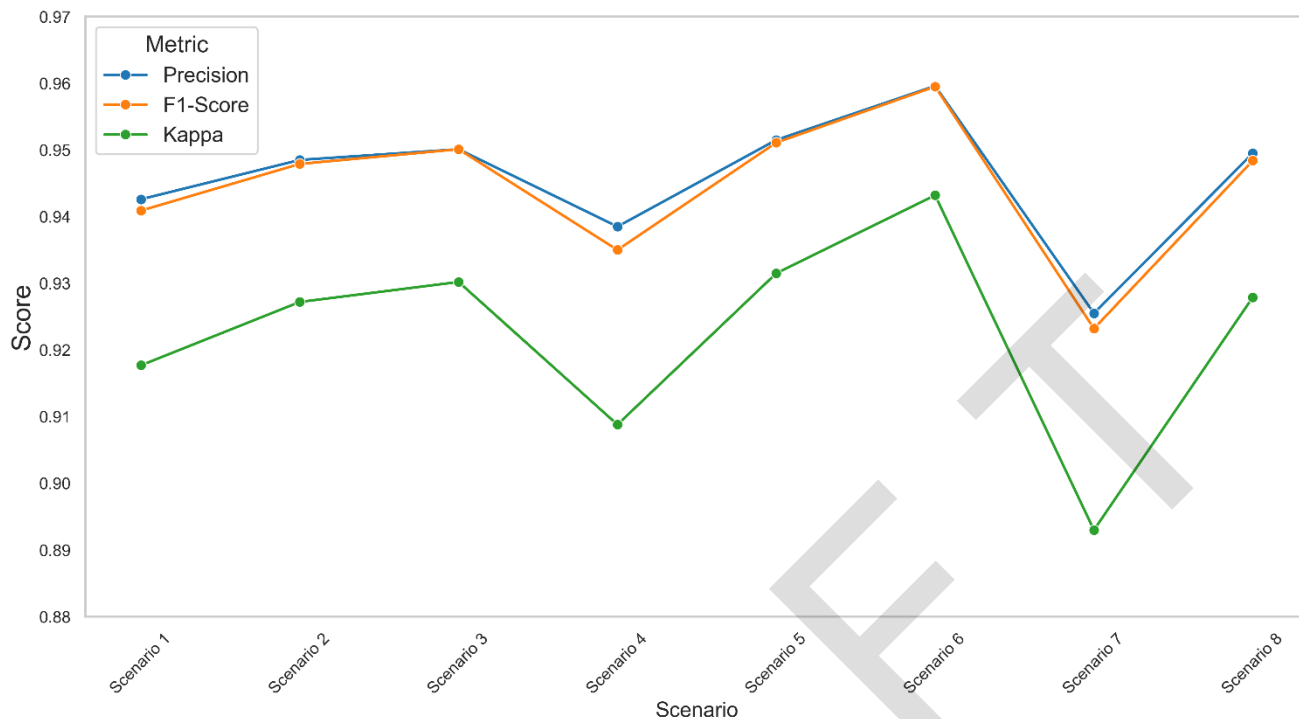


Figure 12. Performance metrics by spatial distribution scenarios (IMLP).

TABLES

Table 1. Comparative aspects of explicit vs. implicit modeling.

Aspect	Explicit Modeling	Implicit Modeling
Respect for drillhole contacts	Yes	Yes
Modeling speed	Slow	Fast
Ability to replicate models	No	Yes
Auditability complexity	High	Low
Level of subjectivity	High	Low
Modeler supervision requirement	High	Low

Table 2. Commercial geological modeling software.

Company	Software	Includes ML	Includes MI
Sequent	Leapfrog GEO	No	Yes
Datamine	Studio RM	No	Yes
Maptek	Vulcan Implicit Modeling	No	Yes
Maptek	Domain MCF	Yes	No
Rock Flow Dynamics	tNavigator Geology	Yes	Yes

Table 3. Drillholes dataset statistics.

	count	mean	std	min	Q1	Q2	Q3	max
X	1320	465.03	317.31	0	137.84	378.45	751.88	1,000.00
Z	1320	150.00	87.36	0	75.00	150.00	225.00	300.00
Rocktype	1320	2.34	1.24	1.00	1.00	2.00	4.00	4.00
SDF _{R1}	1320	26.22	62.01	-85.71	-20.17	12.61	73.11	216.81
SDF _{R2}	1320	66.06	56.34	-25.21	20.17	57.98	108.40	194.38
SDF _{R3}	1320	45.73	52.52	-57.98	5.04	42.86	80.80	181.64
SDF _{R4}	1320	74.38	88.37	-90.76	-2.52	75.63	150.94	242.02
SG	1320	1.97	0.56	1.01	1.40	2.02	2.53	2.70

Table 4. Evaluation of metrics (models vs. real data)

Model	Precision	Recall	F1-Score	Kappa
IM-RBF	0.89	0.88	0.87	0.83
IM-OK	0.87	0.86	0.85	0.80
IMLP	0.96	0.96	0.96	0.94